Observatoire de Paris - PSL

M1 Sciences de l'Univers et Technologies Spatiales

LIU report: the 21 cm H I line in galaxies

Author:
Adrien ANTHORE

Supervisors:
Jean-Michel MARTIN
Wim VAN DRIEL

Lab insertion unit

December 2, 2022

1 Acknowledgements

I would like to thank my supervisors, Jean-Michel Martin and Wim van Driel who made this project possible. They taught me a lot during those weeks and what I have learned will help me a lot in my future work.
I would also like to thank Benoît Mosser who organised the LIU and who gave us the opportunity to work on projects that interest us.
Finally, I would like to thank Cédric Leyrat and Caroline Barban, co-heads of the M1, who are very concerned about our studies, projects and internships.

2 Introduction

This LIU was performed at the GEPI (Galaxies, Étoiles, Physique et Instrumentation) department of Paris Observatory, with Jean-Michel Martin and Wim van Driel as supervisors.
The topic is the study of the 21 cm H I line in galaxies, in particular its role in estimating their Dark Matter content. We observed eight galaxies with the NançayRadio Telescope (NRT) in order to understand the physics behind the observations and the standard tools used.
The first objective was to understand radio astronomical observation techniques with a single dish radio telescope in order to learn about data processing in the context of radio astronomy. The second objective was to learn how to write a scientific paper based on the work I did in the laboratory, which will complete this report.

3 Context

The context is globally presented in the article, but some details of the scientific and technical contexts are developed in this section.

3.1 21 cm H I line

The 21 cm line radiation of neutral atomic hydrogen gas, H I, is due to the hyperfine structure of the hydrogen atom. This radiation occurs when the spin of the nucleus and the electron change from a symmetrical state to an anti-symmetrical state. Its laboratory wavelength is 21 cm, that means a frequency of 1420 MHz.

The study of the H I gas is essential in order to understand the evolution, star formation and dynamics of galaxies.
We chose here to study late type galaxies, that means spiral galaxies. The reason for this choice is that those galaxies still have gas to form new stars, contrary to early type galaxies. Most of the gas inside spiral galaxies is located in the spiral arms. Indeed, in the spiral arms there is still star formation and young stars, that explains why they appears bluer, as very luminous blue stars dominate the luminosity in star forming regions. However, H I disks are larger than stellar disks. In the center of spiral galaxies, in the bulge, there is no star formation. That means that this region is poor in neutral hydrogen gas and the bulge appears more red because older stars tend to be red.
In spiral galaxies, hydrogen represents 90% of the interstellar medium in terms of abundance. Although helium constitutes only 10% of the interstellar medium, it contributes to 40% to the gas mass of the galaxy. The order of magnitude of the mass of the neutral atomic hydrogen gas in an average spiral galaxy is $10^9\ M_\odot$.

Measuring a detailed H I line profile allows us to measure two different total masses of a galaxy: (1) its total dynamic mass, using the Doppler-Fizeau effect to determine the rotation velocity of the galaxy and its H I gas, and (2) its total H I mass, from the distance of the galaxy and its H I flux flux.
As mentioned in the article Section 2, the galaxies observed are edge-on to directly measure their maximum rotation velocity without needing a correcting for inclination.
We expect to see double horned H I profiles with sharp edges for disks with flat rotation curves. The horn with the lower radial velocity will correspond to the gas from the spiral arms rotating toward us and the other one to the gas from the spiral arms rotating away from us.

3.2 Description of the NRT

The observations were performed with the large NRT radio telescope at the Nançay Radio Observatory. As shown in Figure 1, the NRT consists of 3 main elements :

- (1) The primary mirror: $200 \times 40\ m$ plane mirror that can tilt to point at the declination of the target;
- (2) The secondary mirror: spherical mirror that is a $\sim 300 \times 35\ m$ section from a sphere of a radius of 560 m;
- (3) The focal cabin: movable cabin containing the receivers at the focus of the NRT. The supporting track of the cabin is 80 meters long, and a target can be tracked in right ascension for about an hour.

Due to its structure, the beam shape of the NRT is not circular. For the H I line observation ($\lambda = 21\,cm$) we have $\theta_h = \lambda/D_h = 3.6'$ along the horizontal axis (right ascension), and $\theta_v = \lambda/D_v = 23'$ on the vertical axis (declination).
For our observations the raw velocity resolution is $\delta V_r = 2.6\,km/s$, which was later smoothed to 10 km s^{-1} during the data reduction process.

4 Methods used

You will find in Sections 2 and 3 of the article the methods used in terms of galaxy selection, observation and data reduction. In this section, I will give further details about the whole process.
The software used during the LIU were: Linux, to manage the files and data and to have access to the NRT servers; standard NRT software packages NAPS[1] and SIR, to do the data reduction and process the results; Python, to make the computations of a number of parameters (see below).

The first step was to select a sample of galaxies to study. In preparation for the LIU project, my supervisors had requested 11 hours of NRT telescope time. which were allocated allocated by the Time Allocation Committee.

Once the sample was defined, we needed to prepare the observations and inform the operator of the NRT. We created and sent a source file that contains information about each target, especially the coordinates of the target to track during each observation, and the instrumental set-up to be used.
Once an observation was made, we exported the data and we processed them with NAPS and SIR.
The spectrum obtained from the routine shows the flux density as a function of radial velocity. The output data are the noise level, peak signal-to-noise ratio, mean radial velocity, $V_{\rm HI}$, line width at 50% and 20% of the maximum, W_{50} and W_{20} and the integrated line flux, $F_{\rm HI}$(for more details, see Section 4 in the article).
Finally, we used the routine I wrote in Python, which is presented in Annex 7.1, to calculate derived quantities listed in Tables 2 and 3, based on the results we obtained and some parameters taken from databases: uncertainties in line parameters $V_{\rm HI}$ and $F_{\rm HI}$, and global galaxy parameters such as $L_{\rm B}$, $M_\star$, $M_{\rm HI}$, $M_{\rm bar}$, $V_{\rm rot}$, and $M_{\rm tot}$.

[1] http://nrt.obspm.fr/nrt/support/naps/node1.html

Once all the computations have been made, we can compare them to other observations published in the literature (see Figure 2).

5 Discussion

The results are described in Section 4 of the article. In this part, I will add more details on some specific points, and ideas about what I could have done if I had had more time.

First of all, looking at Figure 2 in which we compare the measured parameters that characterize our H I line profiles to those from the literature, we can see that our results are consistent with the literature values, which is good news.
For example, the average difference in central H I line velocities, $V_{\rm HI}$, is -2$\pm$7 km s^{-1}, compared to the NRT velocity resolution of 10 km s^{-1} of our final spectra.

In the observations of the galaxy FGC 1496 we noticed a ripple pattern in the baseline of the spectrum that looks like a well-known stationary wave between large metal structures of the NRT. I tried to use a Fourier transform to remove it but it was more complex than expected. The perturbation had more than one frequency and I did not have time to study in detail its FFT power spectrum in order to find the exact frequency, or frequencies, of the perturbations. My best attempt is shown in figure 3.

Another unexpected feature is that the H I profile of IC 2267 has only one horn and a more gaussian-shaped profile, unlike the double horned profiles of the other galaxies. By looking at its optical image we noticed that the galaxy has a warp and what looks like a tidal filament outside the disk. This may be the sign of a minor interaction that would explain why its profile only has one horn but we can't be sure. For instance, we also see a warp in the optical image of **UGC 7170** but its profile has two horns, as expected.

Finally, the goal was to estimate the dark matter content in the galaxies. It depends on the total dynamic mass and the baryonic mass of the galaxy. The estimation of the baryonic mass was not difficult since we know the contribution of helium and hydrogen gas, and we estimated the stellar mass from other observations.

However, the estimation of the total dynamic mass was more complicated. The formula used was $2.326\,10^5\,{V_{\rm rot}}^2 r_{\rm max}$ where $V_{\rm rot}$ is the maximum rotation velocity estimated from the line widths measured at 20% of the peak level corrected for the inclination of the galaxy, and $r_{\rm max}$ is the radius of the H I distribution. The difficulty was to determine this radius for the observed galaxies, as we did not obtain interferometric imaging in H I. We had to look for a conversion factor between the optical radius and the H I radius of galaxies. We found out from published imaging studies that the H I radius is greater than the optical radius in the *B* band and that it depends on the surface brightness nature of the galaxy observed, LSB or HSB, as detailed in Section 5 of the article.

6 Conclusions

The scientific conclusions of the project can be found in Section 6 of the article. We found out that the dark matter dominates, at the 85% level, the total mass of the galaxies, consistent with literature results.

Here I will conclude on my personal experience of my LIU.

During the LIU, I have learned a lot about galaxies and especially about the physical aspects behind the H I line observations. I also learned a lot about how observations are performed in radio astronomy and how we process data. And I was able to find results and estimate parameters that are coherent with the bibliography.

Another achievement I have made in this LIU is that I learned how we write a scientific paper. It was made on Overleaf in collaboration with my supervisors where all new texts, questions, comments and revisions could be tracked.

All things considered, I learned a lot, not only in terms of scientific knowledge. I am genuinely satisfied of this LIU and I am thankful for having had the opportunity to work on this project.

7 Annex

7.1 Codes

As mentioned, it is used to calculate derived quantities listed in Tables 2 and 3, based on the results we obtained and some parameters taken from databases (see hereafter): uncertainties in line parameters $V_{\rm HI}$ and $F_{\rm HI}$, and global galaxy parameters such as $L_{\rm B}$, $M_\star$, $M_{\rm HI}$, $M_{\rm bar}$, $V_{\rm rot}$, and $M_{\rm tot}$.
The code takes as input for a given galaxy: its name, radial velocity in radio convention, $F_{\rm HI}$, W_{20}, W_{50}, inclination, optical radius D_{25} in units of $0'.1$, *rms* and *SNR* of the observation, total apparent magnitude in the *B* band, Milky-Way absorption in the *V* bandy, and its surface brightness type. It was written in python, all the codes and the documentation are presented on my github : https://github.com/ADnothing/2022_M1LIU

7.2 Figures

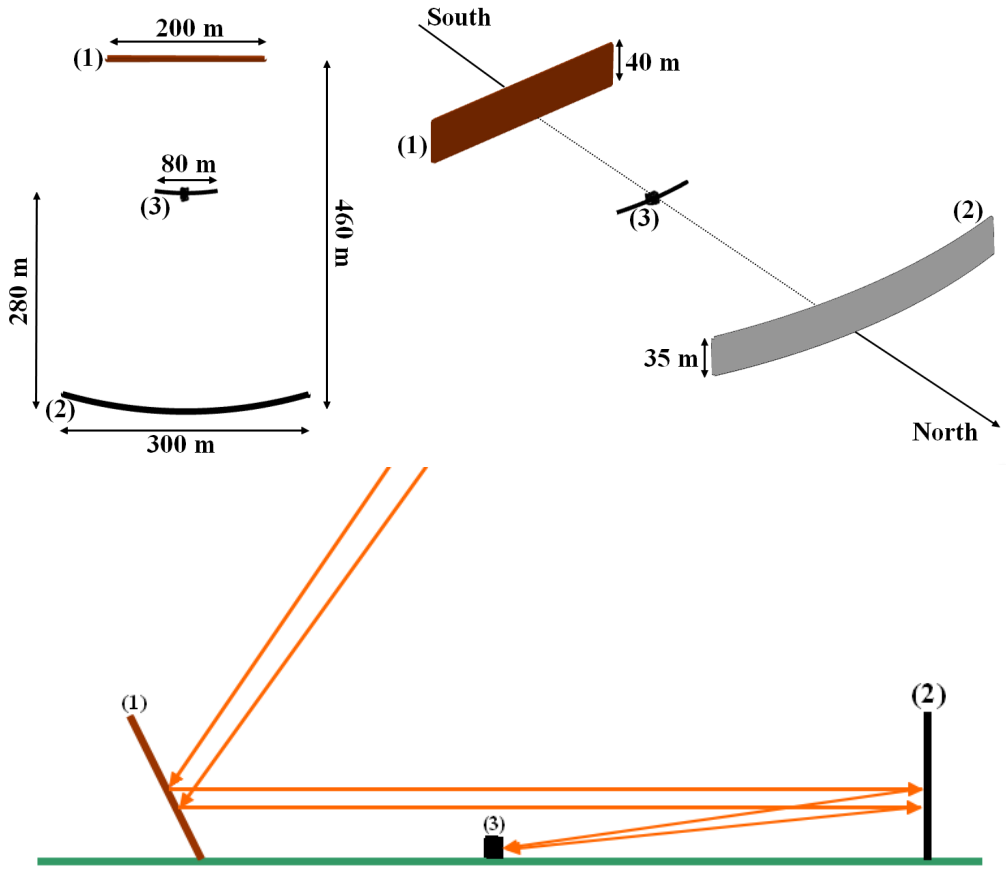

Figure 1: Schematic views of the NRT. Shown here is its structure from different angles. There are 3 main elements: (1) plane mirror, (2) spherical mirror, and (3) focal cabin. The first view (top-left) is the NRT as seen from above. The second view (top right) is a top-sideways view of the telescope, which shows the local N-S meridian as well as the orientation of the NRT. The last is a ground level view, which shows the path of the radio waves from a source to the focus of the NRT.

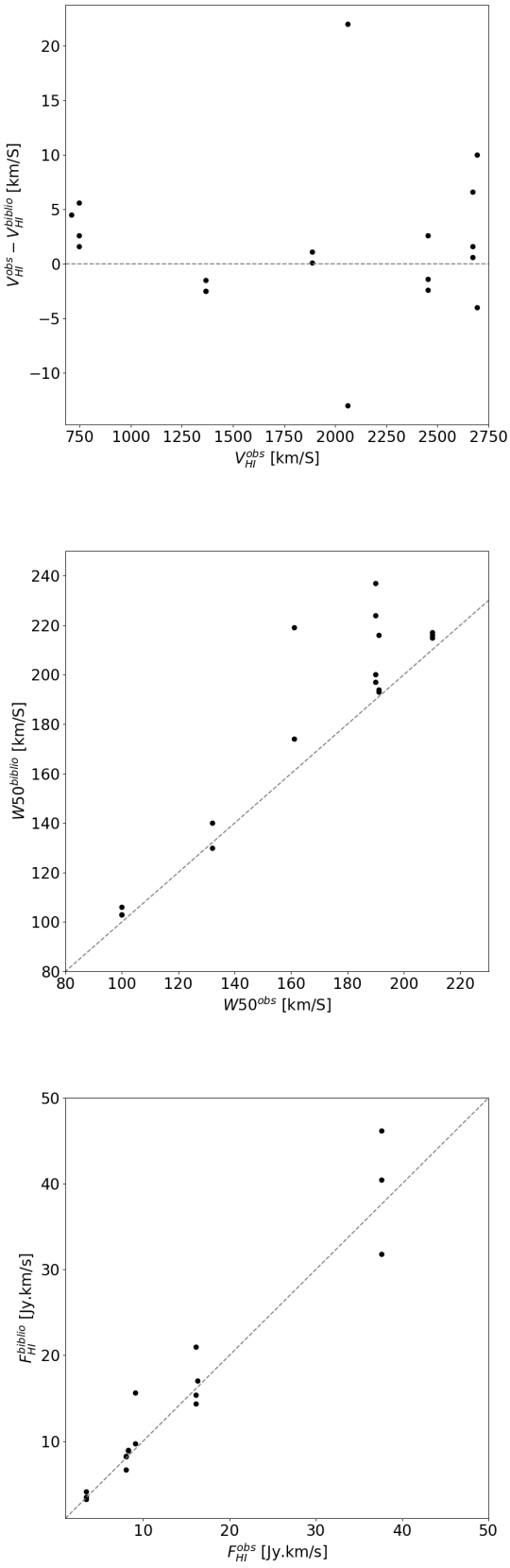

Figure 2: Comparison of the H I line parameters we observed with those from other observations found in the literature. The first plot compares the central radial velocities of the profiles, $V_{\rm HI}$ in km s^{-1}, where differences between our values and literature values are shown as a function of $V_{\rm HI}$, the second plot compares the line widths measured at 50% of the peak level, W_{50} in km s^{-1}, and the third compares the integrated line fluxes, F$_{HI}$ in Jy km s^{-1}. The diagonal lines correspond to $y = x$, and do not represent a fit to the data.

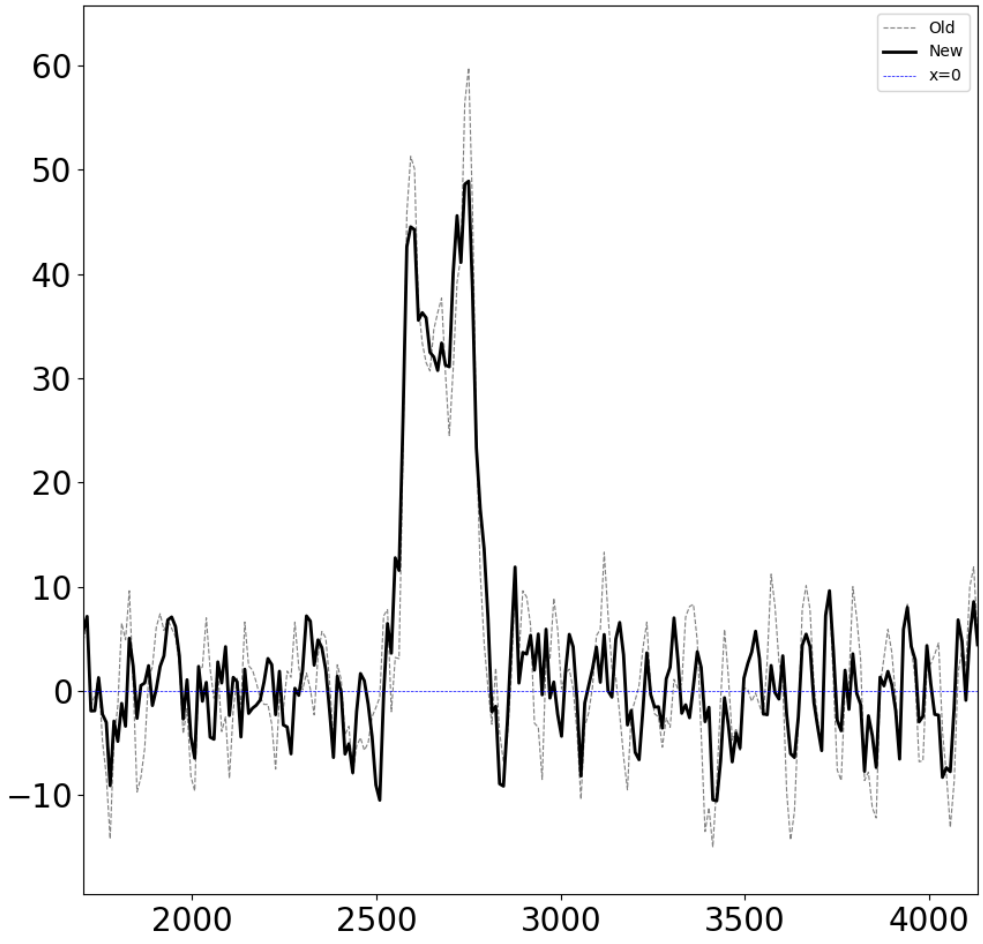

Figure 3: Attempt to remove a standing wave in the baseline of the H I line profile of **FGC 1496**. Shown are flux density (in mJy) as a function of radial velocity (in km s^{-1}). The objective was to identify and remove peaks in the Fourier domain in order to remove the oscillations due to the standing wave pattern. The dashed gray line shows the observed spectrum and the full line the corrected spectrum after removal of FFT components.

Astronomy & Astrophysics manuscript no. output
December 2, 2022

HI line observations of galaxies with the Nançay Radio Telescope

Adrien Anthore[1]

Master Sciences de l'Univers et Technologies Spatiales de l'Observatoire de Paris-PSL: M1 ⋆

ABSTRACT

We have performed 21 cm H I line observations with the 100 m-class single dish Nançay Radio Telescope of six edge-on Low Surface Brightness (LSB) galaxies and two High Surface Brightness (HSB) galaxies, all with previously reported strong H I lines. Using our measured H I line parameters, and optical and H I line imaging data from the literature, we estimated the dark matter content of the observed galaxies. We found that dark matter represents on average 88±4% of the total mass for the LSB galaxies and 73±5% for the HSB galaxies. This result is consistent with previous studies.

Key words. galaxies: general – radio lines: galaxies

1. Introduction

The main goal of this project is to estimate the dark matter contents of a sample of spiral galaxies using 21 cm H I line spectra which we obtained with the single-dish Nançay Radio Telescope (NRT).

For this purpose, we will estimate their total and their baryonic masses; the difference between those two terms corresponds to an invisible mass component in the galaxies, their dark matter. In order to estimate the total mass we need to determine the maximum rotation speed and the radius of the H I distribution of the galaxies. Their baryonic mass is estimated from the mass of gas and stars in the galaxies.

We mainly selected edge-on spiral galaxies from the Flat Galaxies Catalogue (FGC, Karachentsev et al. 1993 with already known strong H I lines (Matthews & van Driel 2000), to ensure their detection within the allocated NRT telescope time and to directly measure their maximum rotation velocity.

Optical surface photometry has shown (e.g. Matthews 2000; Matthews & Uson 2008) that these are Low Surface Brightness (LSBs) galaxies. We adopt the commonly used definition that LSBs have a central surface brightness at least $1 magarcsec^{-2}$ fainter than the surface brightness of the sky. Most LSB galaxies are low mass, low metallicity and rather blue galaxies with a high mass-to-light ratio (O'Neil, K. et al. 2004). We also observed two High Surface Brightness (HSBs) spiral galaxies, the type that defines the Hubble sequence.

Unless otherwise indicated, all radial velocities are heliocentric and in the optical convention, $cz = c(\lambda - \lambda_0)/\lambda_0$. A standard Hubble constant of 70 km s^{-1} Mpc^{-1} was used throughout the paper.

2. Galaxy selection

We selected galaxies which (1) lie within the RA range accessible within the allocated telescope time, (2) lie within the declination range accessible at Nançay, $\delta \geq -39°$, (3) have known strong H I lines, (4) are preferably edge-on, to measure directly their maximum rotation velocity, and (5) are smaller than the telescope beam size.

The final sample consist of eight galaxies, six edge-on late-morphological type (Scd-Sm) LSB galaxies from the FGC, and two HSB spirals, one edge-on (NGC 3600) and another (NGC 7741) with an inclination of 50°, which had been selected when no suitable FGC candidates were available.

Listed in Table 1 are basic optical properties of the observed galaxies. Unless otherwise indicated, the data were taken from the online databases HyperLeda[1] and NED[2].

- RA, Dec: right ascension and declination of the optical center in epoch J2000.0, taken from the NED database;
- Morph.: morphological type taken from NED, or otherwise from the FGC;
- B_T: total apparent magnitude in the B band, within the 25 mag arcsec^{-2} isophote;
- D_{25}: major axis diameter in the B band, at the 25 mag arcsec^{-2} isophotal level, in $'$;
- b/a: minor-to-major axis ratio in the B band, at the 25 mag arcsec^{-2} isophotal level;
- V_{opt}: heliocentric radial velocity of the galaxy, in km s^{-1}.

3. Observations and data reduction

The Nançay Radio Telescope telescope (NRT) is a 100 m-class meridian transit, single dish-type instrument. It consists of a tiltable plan mirror (200 m long and 40 m high), a spherical mirror (300 m long and 35 m high) and a focal cabin which contains the receivers. The telescope beam size is $3'.5 \times 23'$ (alpha times delta). We made observations simultaneously in two linear polarizations in 4096 frequency channels, resulting in a 2.6 km s^{-1} velocity resolution over the radial velocity range -3239 to 7457 km s^{-1} Flux calibration is performed by frequent insertion of a calibrated noise diode into the beam and regular observations of strong continuum radio sources by NRT staff. The data

⋆ Project supervisors: J.-M. Martin and W. van Driel, GEPI, Observatoire de Paris, Université PSL, CNRS, 5 place Jules Janssen, 92195 Meudon, France

[1] http://leda.univ-lyon1.fr/
[2] https://ned.ipac.caltech.edu

Table 1. Basic optical properties of the observed galaxies

Name	RA (J2000.0)	Dec	Morph.	B_T (mag)	D_{25} (′)	b/a	V_{opt} (km/s)	reference
IC 2267	08 18 01.5	24 44 10	SBcd?	15.20	1.9	0.13	2083	Aihara et al. (2011)
NGC 3600	11 15 52.0	41 35 27	Sa?	12.98	1.9	0.32	703	Alam et al. (2015)
UGC 7170	12 08 04.0	19 06 05	Scd:	14.73	2.8	0.08	2443	Alam et al. (2015)
FGC 1496	12 44 19.1	-05 32 13	Sd:	15.90	1.7	0.10		
FGC 1543	13 02 55.7	55 41 40	Sm	17.04	0.9	0.18	1357	Alam et al. (2015)
ESO 577-038	13 48 25.7	-18 52 20	Sd:	16.61	2.1	0.05		
FGC 1731	14 14 34.1	-04 25 02	Sd	16.50	1.0	0.15		
NGC 7741	23 43 54.4	26 04 32	SBcd	11.82	3.6	0.66	750	Blackman & Pence (1982)

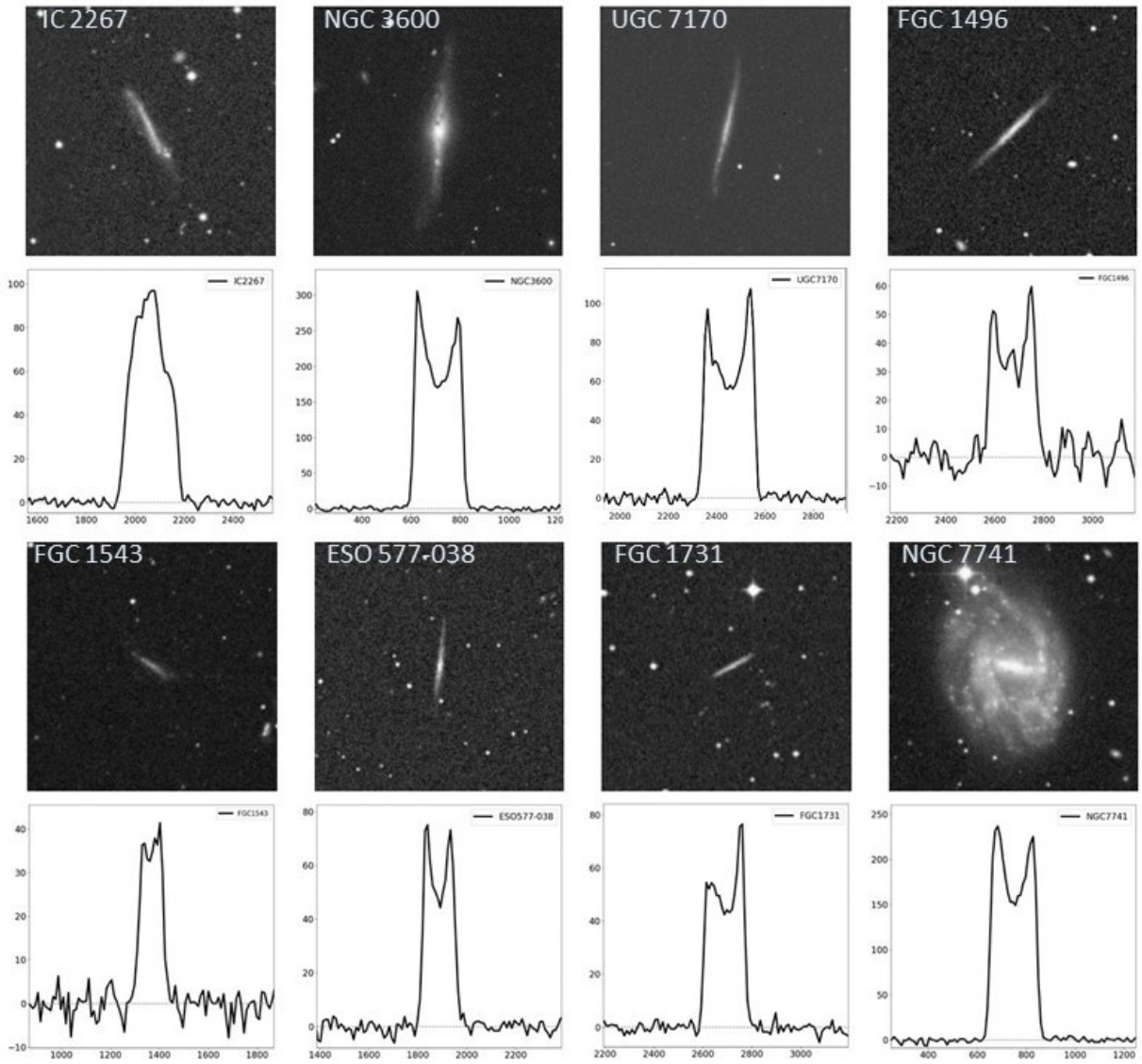

Fig. 1. Pairs of optical images and our Nançay 21 cm H I line spectra for each of the observed galaxies. The optical images are digitized photographic plates in the *B* band from the Digital Sky Survey DSS2, of $5' \times 5'$ in size. The corresponding H I profiles show flux density (in mJy) as a function of radial velocity (in km s^{-1}).

were taken in an equal integration time, on/off-source position-switching mode. The observations were made in October 2022, using a total of about 20 hours of telescope time.

We used standard NRT software SIR to (1) average the data obtained in the two receiver polarizations, (2) convert signal strengths from system temperature to flux density in mJy, (3) fit and subtract polynomial baselines, (4) smooth the data in velocity to a resolution of 10 km s^{-1}, and (5) convert the radial H I velocities (V_{radio}), measured based on frequencies, to the standard optical cz convention (V_{HI}), as $cz = 1/((1/V_{radio}) - (1/c))$ (for further technical details see e.g. van Driel, W. et al. 2016).

Table 2. H I line profile parameters of the observed galaxies

Name	*rms* (mJy)	*SNR*	V_{HI} (km/s)	W_{50} (km/s)	W_{20} (km/s)	F_{HI} (Jy km/s)
IC 2267	1.45	67	2061.0±0.9	190	230	16.3±0.2
NGC 3600	2.34	130	708.5±0.2	199	215	45.6±0.3
UGC 7170	1.91	56	2453.4±0.5	210	229	16.1±0.2
FGC 1496	5.87	10	2671.4±3.1	190	211	8.0±0.6
FGC 1543	2.64	16	1367.5±2.2	100	122	3.4±0.2
ESO 577-038	2.33	32	1886.9±0.9	132	151	8.3±0.2
FGC 1731	1.86	41	2693.0±0.7	161	180	9.1±0.2
NGC 7741	2.47	95	747.4±0.3	191	209	37.6±0.3

Table 3. Estimated global parameters of the observed galaxies

Name	d (Mpc)	$\log(L_B)$ ($L_{\odot,B}$)	$\log(M_\star)$ ($M_\odot$)	$\log(M_{HI})$ ($M_\odot$)	$\log(M_{bar})$ ($M_\odot$)	V_{rot} (km/s)	$\log(M_{tot})$ ($M_\odot$)	M_{tot}/M_{bar}	$DM\%$
IC 2267	29.9	9.11	9.26	9.54	9.82	115	10.79	9	89
NGC 3600	12.6	9.23	9.38	9.23	9.68	108	10.17	3	68
UGC 7170	36.6	9.47	9.62	9.71	10.05	113	11.04	10	90
FGC 1496	38.6	9.05	9.19	9.45	9.74	106	10.80	12	91
FGC 1543	23.2	8.13	8.27	8.63	8.89	61	9.80	8	88
ESO 577-038	27.0	8.54	8.69	9.15	9.39	76	10.44	11	91
FGC 1731	39.6	8.84	8.99	9.53	9.75	90	10.42	5	79
NGC 7741	12.3	9.75	9.90	9.12	9.99	136	10.65	5	78

4. Results

The H I profiles and optical *B* band images of the observed galaxies are shown in Fig. 2.

Listed for each galaxy in Table 2 are the following parameters of their H I line profiles:

- *rms*: rms noise level of the spectrum, in mJy;
- *SNR*: peak signal-to-noise ratio, i.e., the peak flux density divided by the *rms*;
- V_{HI}: mean radial velocity, in km s^{-1};
- W_{50}: line width at 50% of the peak level, in km s^{-1};
- W_{20}: line width at 20% of the peak level, in km s^{-1};
- F_{HI}: integrated line flux, in Jy km s^{-1}.

The uncertainties in V_{HI} and F_{HI} were estimated following Schneider et al. (1990). Uncertainties in W_{50} and W_{20} are, respectively, 2 and 3.1 times those in V_{HI}.

$$\sigma_{V_{HI}} = 1.5(W_{20} - W_{50})/(SNR) \quad (1)$$

$$\sigma_{F_{HI}} = 2.810^{-3} {W_{20}}^{0.5} R^{0.5} rms \quad (2)$$

Where R is the velocity resolution of the spectra, in km s^{-1}.

Listed for each galaxy in Table 3 are our estimated global parameters. For further details on the methodology used, see Section 5.

- d: distance of the galaxy (in Mpc), based on its radial velocity corrected for the infall of the Local Group toward the Virgo cluster and using the Hubble-Lemaître law with a Hubble constant H_0 = 70 km s^{-1} Mpc^{-1};
- L_B: total luminosity in the *B* band (in $L_{\odot,B}$) calculated using B_T corrected for Galactic foreground extinction following Schlafly & Finkbeiner (2011), and assuming a *B* band solar absolute magnitude of 5.48 mag (Allen 1973);
- $M_\star$: total stellar mass (in $M_\odot$), estimated from L_B using a mass-to-luminosity conversion factor of 1.4 $M_\odot/L_{\odot,B}$;
- M_{HI}: total H I mass (in $M_\odot$), $M_{HI} = 2.35610^5 d^2 F_{HI}$;
- M_{bar}: total baryonic mass (in $M_\odot$), $M_{bar} = M_\star + 1.4M_{HI}$;
- V_{rot}: maximum rotation velocity (in km s^{-1}), $V_{rot} = W_{20}/2\sin(i)$;
- M_{tot}: total (dynamical) mass, $M_{tot} = 2.32610^5 {V_{rot}}^2 r_{max}$;
- $DM\%$: percentage of the dark matter contribution to the total mass.

5. Discussion

Distances d were calculated using radial velocities corrected for the infall of the Local Group towards the Virgo cluster, as listed in HyperLeda, and adopting a Hubble constant of H_0 = 70 km s^{-1} Mpc^{-1}. This correction was applied because for galaxies close to the Milky Way local kinematics can have a significant impact on their observed radial velocities. In three cases the corrections were significant, 14-25%

To compute L_B luminosities we did not use the *btc* values from HyperLeda, which are total apparent magnitudes in the *B* band corrected for the extinction due to both the dust inside the galaxy itself as well as in the Milky Way. This correction of on average a factor 5 in luminosity, which was estimated for HSB galaxies, appears significantly overestimated for our galaxies, most of which are LSBs and for which we do not see much dust in optical images (see Fig. 2). The total apparent magnitude we have used therefore includes only a correction to B_T for the Galactic extinction, A_B, estimated as $1.32A_V$ Cardelli et al. (1989) where A_V is the Galactic extinction in the *V* band, as listed in NED.

To estimate the total stellar mass $M_\star$ we used the *B*-band stellar population mass-to-light ratio of 1.4 $M_\odot/L_{\odot,B}$ adopted by McGaugh et al. (2000).

The total baryonic mass $M_{\rm bar}$ was approximated as the sum of $M_\star$ and the total gas mass, which was assumed to be 1.4 times the total H I mass, a standard correction factor to account for Helium gas. We did not take into account the molecular hydrogen gas mass, as it does not appear to be significant in late type galaxies (McGaugh et al. 2000).

The total (dynamical) mass $M_{\rm tot}$ was calculated assuming a simple spherical distribution of dark matter around the galaxy. For the maximum rotation speed $V_{\rm rot}$ of the flat part of the rotation curve of a galaxy we used the common assumption that it corresponds to the W_{20} line width, corrected for the inclination, We based our estimates for the $r_{\rm max}$ radii of the H I distributions on the optical radii of galaxies and their relationship with the radii of their H I distributions, as derived from interferometric H I line imaging observations. For this, the surface brightness nature of the galaxies was taken into account, as the ratio of H I-to-optical radii is different for LSB and HSB galaxies. The H I diameter of a galaxy is measured where its radially averaged H I surface density reaches the 1 $M_\odot/pc^2$ level, and its optical isophotal diameter R_{25} is based on D_{25} measured at the 25 mag arcsec^{-2} level in the B band. To determine $r_{\rm max}$ we adopted the following average ratios for the H I-to-optical radii: 2.5±1.1 for LSB galaxies (de Blok et al. 1996) and 1.6±0.3 for HSB galaxies (Rhee & van Albada 1996).

6. Conclusions

We estimated the dark matter contents of eight galaxies using 21cm H I line spectra we obtained with the single-dish NRT. We found that the estimated dark matter component dominates their total mass at the 85% level, a result which is consistent with other estimates (e.g., de Blok et al. 1996; Rhee & van Albada 1996).

The main sources of uncertainty in our dark matter mass estimates are (1) that the 3D distribution of dark matter around galaxies is not (well) known, which led to our use of an overly simplified formula for the estimation of the total mass (as other studies have done, perforce), and (2) the H I distribution radius $r_{\rm max}$, estimated based on average values measured from interferometric H I line imaging of other galaxies.

References

Aihara, H., Allende Prieto, C., An, D., et al. 2011, ApJS, 193, 29
Alam, S., Albareti, F. D., Allende Prieto, C., et al. 2015, ApJS, 219, 12
Allen, C. W. 1973, Astrophysical quantities
Blackman, C. P. & Pence, W. D. 1982, MNRAS, 198, 517
Cardelli, J. A., Clayton, G. C., & Mathis, J. S. 1989, ApJ, 345, 245
de Blok, W. J. G., McGaugh, S. S., & van der Hulst, J. M. 1996, MNRAS, 283, 18
Karachentsev, I. D., Karachentseva, V. E., & Parnovskij, S. L. 1993, Astronomische Nachrichten, 314, 97
Matthews, L. D. 2000, The Astronomical Journal, 120, 1764
Matthews, L. D. & Uson, J. M. 2008, AJ, 135, 291
Matthews, L. D. & van Driel, W. 2000, A&AS, 143, 421
McGaugh, S. S., Schombert, J. M., Bothun, G. D., & de Blok, W. J. G. 2000, The Astrophysical Journal, 533, L99
O'Neil, K., Bothun, G., van Driel, W., & Monnier Ragaigne, D. 2004, A&A, 428, 823
Rhee, M. H. & van Albada, T. S. 1996, A&AS, 115, 407
Schlafly, E. F. & Finkbeiner, D. P. 2011, ApJ, 737, 103
Schneider, S. E., Thuan, T. X., Magri, C., & Wadiak, J. E. 1990, ApJS, 72, 245
van Driel, W., Butcher, Z., Schneider, S., et al. 2016, A&A, 595, A118